# Synthetic Control to Achieve Lanthanide(III)/Pyrimidine-4,6-dicarboxylate Compounds by Preventing Oxalate Formation: Structural, Magnetic, and Luminescent Properties

Javier Cepeda,*[†] Rolindes Balda,[‡] Garikoitz Beobide,[†] Oscar Castillo,*[†] Joaquín Fernández,[‡] Antonio Luque,[†] Sonia Pérez-Yáñez,[†] and Pascual Román[†]

[†]Departamento de Química Inorgánica, Facultad de Ciencia y Tecnología, Universidad del País Vasco, UPV/EHU, Apartado 644, E-48080 Bilbao, Spain

[‡]Departamento de Física Aplicada I, Escuela Superior de Ingenieros, Universidad del País Vasco, UPV/EHU, E-48013 Bilbao, Spain

S *Supporting Information*
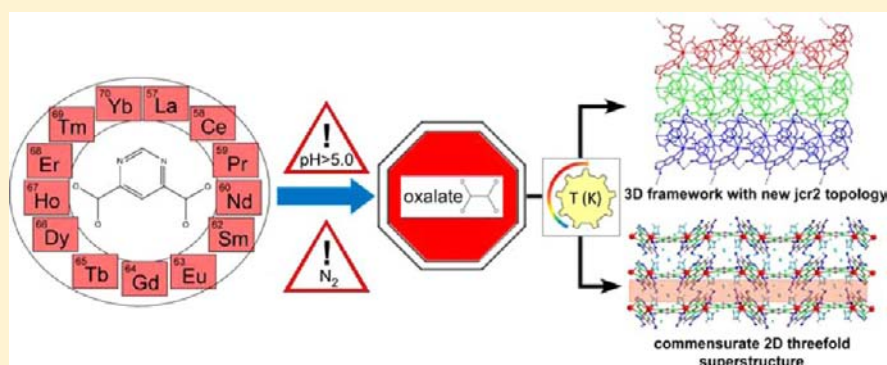
ABSTRACT: Control over the synthetic conditions in many metal/diazinedicarboxylato systems is crucial to prevent oxalate formation, since dicarboxylato ligands easily undergo degradation in the presence of metal salts. We report here an efficient route to obtain oxalato-free compounds for the lanthanide/pyrimidine-4,6-dicarboxylato (pmdc) system on the basis of the reaction temperature and nonacidic pH or oxygen free atmosphere. Two different crystal architectures have been obtained: $\{[Ln(\mu\text{-}pmdc)_{1.5}(H_2O)_3]\cdot xH_2O\}_n$ (**1-Ln**) and $\{[Ln_2(\mu_4\text{-}pmdc)_2(\mu\text{-}pmdc)(H_2O)_2]\cdot H_2O\}_n$ (**2-Ln**) with Ln(III) = La−Yb, except Pm. Both crystal structures are built from distorted two-dimensional honeycomb networks based on the recurrent double chelating mode established by the pmdc. In compounds **1-Ln**, the tricapped trigonal prismatic coordination environment of the lanthanides is completed by three water molecules, precluding a further increase in the dimensionality. Crystallization water molecules are arranged in the interlamellar space, giving rise to highly flexible supramolecular clusters that are responsible for the modulation found in compound **1-Gd**. Two of the coordinated water molecules are replaced by nonchelating carboxylate oxygen atoms of pmdc ligands in compounds **2-Ln**, joining the metal−organic layers together and thus providing a compact three-dimensional network. The crystal structure of the compounds is governed by the competition between two opposing factors: the ionic size and the reaction temperature. The lanthanide contraction rejects the sterically hindered coordination geometries whereas high-temperature entropy driven desolvation pathway favors the release of solvent molecules leading to more compact frameworks. The characteristic luminescence of the Nd, Eu, and Tb centers is improved when moving from **1-Ln** to **2-Ln** compounds as a consequence of the decrease of the O−H oscillators. The magnetic properties of the compounds are dominated by the spin−orbit coupling and the ligand field perturbation, the exchange coupling being almost negligible.

■ INTRODUCTION

The rapidly expanding field of crystal engineering of two- and three-dimensional coordinated polymers is of great current interest for both the structural and topological novelty as well as for their potential application as functional materials.[1] Among the diverse metal−organic frameworks, lanthanide based crystal structures are attractive, owing to their unique optical and magnetic properties arising from 4f electrons and characteristic coordination preferences.[2] In particular, the luminescent Ln-MOFs may undertake a dual role by combining the light emission properties with microporosity, magnetism, sensing, and activity as multimodal imaging contrast agents.[3] Compared to first-row transition metal ions, lanthanide ions possess more flexible and larger coordination geometries, which makes it difficult to predict the resulting crystal structure.[4] In principle, these characteristics result in more facile routes to densely packed solids given the trend of the lanthanide atoms

to coordinate to several ligands, although an exhaustive control of the synthetic conditions may direct the assembling toward open architectures due to the important role played by water molecules as terminal ligands.[5] In addition, according to the hard−soft acid−base principle,[6] the lanthanide atoms have high affinity for oxygen donor atoms, which explains the wide variety of reported compounds with a multycarboxylate ligand.[7] Nevertheless, mixed O- and N-donor molecules give the opportunity to discover new polymeric structures with higher complexity due to the bonding through both nitrogen or carboxyl oxygen species.[8]

The carboxylate groups in the 4- and 6-positions of the pyrimidinic ring avoids the steric hindrance between them and confers a planar topology to the pyrimidine-4,6-dicarboxylate dianion (pmdc). This structural feature favors its bis-chelating mode, but even higher connectivity is also available through its uncoordinated carboxylate oxygen atoms; hence, it has a strong potential to build up highly ordered extended structures.[9] On the other hand, our previous experimental work with this ligand under hydrothermal conditions has revealed that its *in situ* partial decomposition generates oxalate anions in the reaction media.[10] The present work is a new contribution to our research on trivalent metal centers and diazinedicarboxylato ligands based systems.[8c,10] It reports an exhaustive study of the synthesis conditions that has allowed us to preclude the decomposition of pmdc, leading to two families of oxalate-free extended Ln/pmdc networks ranging from two-dimensional (2D) sheets (**1-Ln**) to compact three-dimensional (3D) networks (**2-Ln**). All compounds have been structurally and magnetically characterized, while the luminescence properties of some of these compounds have been also accomplished. Furthermore, the use of Fourier-transform infrared (FTIR) spectroscopy has enabled us to get deeper insights into the coordination mode of the pmdc ligand, and it even has allowed distinguishing between the two families of Ln/pmdc compounds. The structural diversity has been rationalized according to the close relationship encountered between the entropy driven hydrothermal desolvation pathway and the combination of ligand steric hindrance and Ln(III) ion size effect.

■ EXPERIMENTAL PROCEDURES

Chemicals. All the chemicals were of reagent grade and were used as commercially obtained. The starting material pyrimidine-4,6-dicarboxylic acid (H_2pmdc) was prepared following the previously reported procedure.[11]

Physical Measurements. Elemental analyses (C, H, N) were performed on an Euro EA elemental analyzer, whereas the metal content, determined by inductively coupled plasma (ICP-AES) was performed on a Horiba Yobin Yvon Activa spectrometer. The IR spectra (KBr pellets) were recorded on a FTIR 8400S Shimadzu spectrometer in the $4000-400$ cm^{-1} spectral region. Magnetic measurements were performed on polycrystalline samples of the complexes with a Quantum Design SQUID susceptometer covering the temperature range 5.0−300 K at a magnetic field of 1000 G. The susceptibility data were corrected for the diamagnetism estimated from Pascal's Tables,[12] the temperature-independent paramagnetism, and the magnetization of the sample holder. Thermal analyses (TG/DTA) were performed on a TA Instruments SDT 2960 thermal analyzer in a synthetic air atmosphere (79% N_2/21% O_2) with a heating rate of 5 °C·min^{-1}. The emission measurements were performed at room temperature in a backscattering arrangement by using the frequency triplet output (355 nm) of a 10 Hz, Q-switched Nd:YAG laser (pulse duration 40 ps) and a Ti-sapphire ring laser in the 770−920 nm spectral range as exciting sources. The emission from the free sample surface was collected along the backward direction of the incident

pump beam with an optical fiber by use of two lenses. The fluorescence was analyzed by using a spectrometer (CVI Spectral Products SM-240) in the VIS and a Hamamatsu C9913GC in the near-infrared. Long-pass filters (Semrock LP355 and LP830) were used to remove light at the pump frequency. Lifetime measurements were performed by exciting the samples with the frequency triplet output (355 nm) of a 10 Hz, Q-switched Nd:YAG laser and detecting the emission with a fast photodiode connected to a digital oscilloscope.

Synthesis of {[Ln(μ-pmdc)$_{1.5}$(H$_2$O)$_3$]·xH$_2$O}$_n$ (x = 5.5, except 6.5 for Gd) [1-Ln; Ln(III) = La, Ce, Pr, Nd, Sm, Eu, Gd, Tb, Dy, Ho, Er, Tm, Yb]. 0.150 mmol of the corresponding metal salt dissolved in 5 mL of water was added dropwise over 25 mL of a water−methanol (1:2) solution containing H_2pmdc (0.0459 g, 0.225 mmol). The resulting solution, with a pH = 2.0−2.5, was kept under vigorous stirring for five hours at room temperature. The resulting precipitates, corresponding to compounds **1-Ln**, were collected by filtration, washed with water and ethanol, and air-dried. Yield: 80−85%. Despite the low crystallinity shown by compounds **1-La**, **1-Ce**, and **1-Pr**, their IR spectra contain all the characteristic bands of the isostructural series (Supporting Information). Colorless square prismatic single crystals of **1-Sm**, **1-Eu**, **1-Gd**, **1-Tb**, **1-Dy**, and **1-Yb** appeared in mother liquid after one week at room temperature.

Synthesis of {[Ln$_2$(μ_4-pmdc)$_2$(μ-pmdc)(H$_2$O)$_2$]·H$_2$O}$_n$ [2-Ln; Ln(III) = La, Ce, Pr, Nd, Sm, Eu, Gd, Tb, Dy, Ho, Er, Tm, Yb]. The compounds were obtained by preparing a water solution (25 mL) containing 0.1 mmol of the metal salt and 0.2 mmol of H_2pmdc (0.0408 g), setting the pH = 5−6 by the addition of NaOH (1 M), placing it onto a 45 mL Teflon-lined stainless steel autoclave under autogenous pressure at 180−200 °C for 3 days (180 °C for La−Nd and 200 °C for Sm−Yb), and then, slowly cooling to room temperature (2 °C/h). Yield: 85−90%. Compounds **2-Ln** can also be synthesized performing the synthesis under inert conditions without prior basification with NaOH, as will be later discussed.

The synthesis at lower temperatures under the latter conditions allows obtaining the new compounds: [Ln(pmdc)$_{1.5}$(H$_2$O)]·xH$_2$O (**A**, La), [Ln(pmdc)$_{1.5}$(H$_2$O)$_2$]·xH$_2$O (**B**, Sm), [Ln-(pmdc)$_{1.5}$(H$_2$O)$_2$]·xH$_2$O (**C**, Sm, Dy, Yb), and [Ln-(pmdc)$_{1.5}$(H$_2$O)$_{2.5}$]·xH$_2$O (**D**, Dy, Yb); which have been characterized by means of elemental analyses, IR spectra, thermogravimetric (TG) measurements, and X-ray powder diffraction (XRPD) measurements (see Supporting Information). Their amount of coordinated water molecules has been estimated as the molecules released at temperatures above 90−100 °C in the TG curves. The crystallization molecules cannot be reliably estimated, since they are lost from room temperature.

X-ray Diffraction Data Collection and Structure Determination. Single crystal diffraction data were collected at 100(2) K on Oxford Diffraction Xcalibur ($\lambda_{MoK\alpha}$ = 0.71073 Å for **1-Gd** and **1-Sm**) and Agilent Technologies Supernova diffractometers ($\lambda_{CuK\alpha}$ = 1.5418 Å for **1-Tb** and **2-Ce**; $\lambda_{MoK\alpha}$ = 0.71073 Å for **1-Eu**, **1-Gd**, **1-Dy**, **1-Yb**, and **2-La**). The data reduction was done with the CrysAlisPro program.[13] Crystal structures of compounds **1-Ln** and **2-Ln** (except for that of **1-Gd**) were solved by direct methods using the *SIR92* program[14] and refined by full-matrix least-squares on F^2 including all reflections (*WINGX* and *Jana2006* for **1-Ln** and **2-Ln**, respectively).[15−17] During the data reduction process it became clear that all the crystal specimens of compounds **1-Ln** were pseudomerohedric twins with a twin law: ($\overline{1}$00/0$\overline{1}$0/001). The final results showed a percentage for the minor domain of 49.1% (**1-Sm**), 42.7% (**1-Eu**), 42.3% (**1-Tb**), 49.6% (**1-Dy**), and 48.0% (**1-Yb**). These compounds present a strong pseudosymmetry, precluding an anisotropic refinement of the nonmetallic atoms of **1-Dy** and **1-Yb**. In compound **1-Gd**, the CCD images obtained at 100 K showed that, in addition to the main reflections, the diffraction pattern also contained weak satellite reflections that could be indexed with four integers as **H** = ha* + kb* + lc* + mq with **q** = (0, $^1/_3$, 0) (see the Supporting Information). Similar, but not well-resolved, diffuse scattering was also found for the remaining compounds of the **1-Ln** family. Therefore, the structures of these compounds were resolved ignoring this diffuse scattering, except for compound **1-Gd**, which has been considered to be commensur-
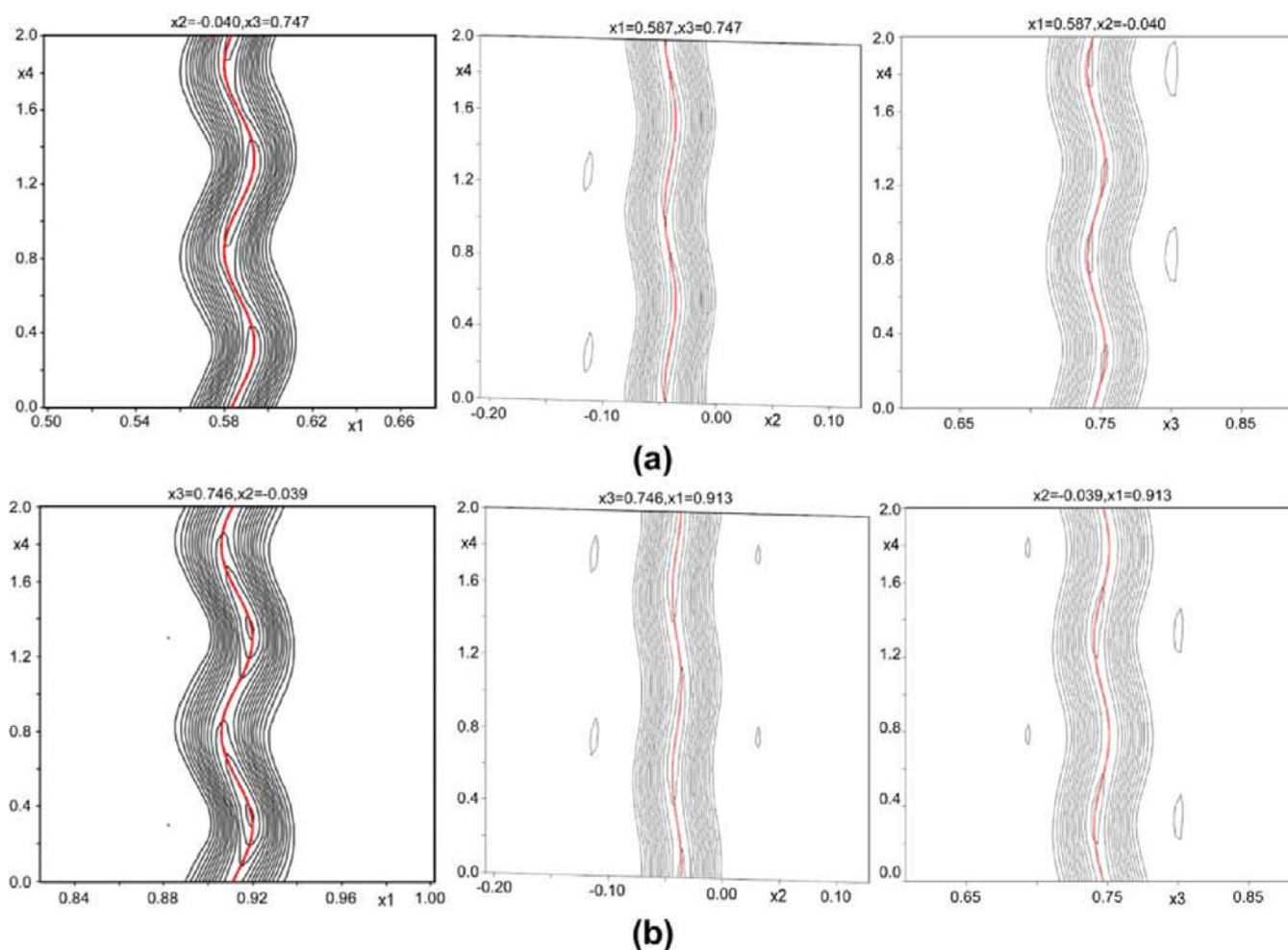
Figure 1. Representation of the atomic modulation function at sections through the electron density at the position of: (**a**) Gd1 and (**b**) Gd2 atoms in compound **1-Gd**.

ately modulated with an *a* X *3b* X *c* supercell and solved in the direct space using the basic cell and the initial structure model provided by the isostructural compound **1-Sm**. Then, it was refined by full-matrix least-squares on *F* by using the *JANA2006* program, which smoothly converged it to a stable solution. The structure model was further improved by adding harmonic positional modulation waves for all the atoms and a modulation wave for the anisotropic displacement parameters (ADP) of the metal atoms. Finally, the twin law was added leading to a percentage of twinned component of 9.30%. After averaging the electron density according to the superspace symmetry, we obtained a good estimate of both the basic positions of the atoms and their modulation functions (Figure 1). During the final steps of refinement high residual electron density was found near the atom O8w, so it was considered to be disordered (O8w′) into two different positions. The disorder was treated introducing a similarity restriction that forces both atoms to possess the same ADP parameters and their occupancies to be complementary modulated.

During the refinement of crystal structures of compounds **2-Ln**, the ADP parameters of several atoms became not positive definite due to the strong pseudosymmetry present. To overcome this problem, a rigid model was applied to the pmdc molecule in such a way that a unique molecule describes the three independent ligands, although independent ADP parameters are employed to refine the thermal movement of each atom. Details of the structure determination and refinement of all compounds are summarized in Tables 1−2.

The XRPD patterns were collected on a Phillips X'PERT powder diffractometer with Cu Kα radiation (λ = 1.5418 Å) over the range 5 < 2θ < 50° with a step size of 0.02° and an acquisition time of 2.5 s per step at 25 °C. Indexation of the diffraction profiles were made by means of the *FULLPROF* program (pattern-matching analysis)[18] on the basis of the space group and the cell parameters found for isostructural compounds by single crystal X-ray diffraction. The unit cell parameters obtained in the final refinement are listed in Tables 1−2. Variable-temperature X-ray powder diffraction measurements of compounds **1-Eu** and **2-Pr** were run under ambient atmosphere with heating rates of 5 °C·min^{-1} and measuring a complete diffractogram every 20 °C.

■ RESULTS AND DISCUSSION

Control Over the pmdc Decomposition to Oxalate. The feasibility to crystallize a wide diversity of compounds upon reaction between the lanthanides and the pmdc ligand, as arises from our previous work on Ln/pmdc/ox[10] and from the herein reported Ln/pmdc systems, highlights the importance of understanding the synthetic conditions that lead to the formation of each of them. The pmdc ligand tends to undergo degradation in the presence of lanthanide salts under hydrothermal conditions rendering oxalate as final product, which easily incorporates to the solid coordination polymer. The present work explores the effect of the reaction conditions, such as the temperature, pretreatment, pH, and atmosphere to prevent the pmdc decomposition in order to crystallize oxalate-free Ln/pmdc compounds (Scheme 1).

The *in situ* generation of oxalate anion under hydrothermal conditions is a commonly reported reaction[19] for systems

Table 1. Crystallographic Data and Structure Refinement Details of Compounds 1-Ln

	1-Nd	1-Sm	1-Eu	1-Gd	1-Tb
empirical formula	$C_9H_{26}N_3NdO_{14.5}$	$C_9H_{26}N_3O_{14.5}Sm$	$C_9H_{26}EuN_3O_{14.5}$	$C_9H_{28}GdN_3O_{15.5}$	$C_9H_{26}N_3O_{14.5}Tb$
formula weight	552.55	558.67	560.28	583.58	567.24
crystal system	monoclinic	monoclinic	monoclinic	monoclinic	monoclinic
space group	$P2_1/c$	$P2_1/c$	$P2_1/c$	$P2_1/c(0\backslash\beta0)s0$	$P2_1/c$
a (Å)	22.753(3)	22.641(1)	22.601(2)	22.577(6)	22.604(1)
b (Å)	11.965(2)	11.933(1)	11.881(1)	11.905(2)	11.847(1)
c (Å)	14.465(3)	14.522(1)	14.441(1)	14.423(6)	14.375(1)
β (deg)	90.67(1)	91.371(3)	91.293(6)	91.35(3)	90.920(4)
V (Å^3)	3937.4(8)	3922.4(5)	3876.7(3)	3875.4(2)	3849.0(5)
GOF^a	–	1.17	1.12	2.13^e	1.08
R_{int}	–	0.0530	0.0440	0.1101	0.0970
χ^2	1.02	–	–	–	–
final R indices					
$[I > 2\sigma(I)]^b$ $R1^c/wR2^d$		0.0543/0.1521	0.0546/0.1403	0.0871/0.1091	0.0825/0.2570
all data $R1^c/wR2^d$		0.0591/0.1491	0.0650/0.1462	0.1504/0.1206	0.0978/0.2711

	1-Dy	1-Ho	1-Er	1-Tm	1-Yb
empirical formula	$C_9H_{26}DyN_3O_{14.5}$	$C_9H_{26}HoN_3O_{14.5}$	$C_9H_{26}ErN_3O_{14.5}$	$C_9H_{26}N_3O_{14.5}Tm$	$C_9H_{26}N_3O_{14.5}Yb$
formula weight	553.68	573.25	575.57	577.25	581.35
crystal system	monoclinic	monoclinic	monoclinic	monoclinic	monoclinic
space group	$P2_1/c$	$P2_1/c$	$P2_1/c$	$P2_1/c$	$P2_1/c$
a (Å)	22.595(2)	22.806(3)	23.058(3)	22.913(3)	22.568(1)
b (Å)	11.832(1)	11.975(1)	12.293(2)	11.988(1)	11.817(1)
c (Å)	14.343(2)	14.475(2)	14.535(2)	14.413(1)	14.220(1)
β (deg)	91.026(1)	90.72(1)	90.71(2)	90.74(1)	90.446(7)
V (Å^3)	3833.9(7)	3953.1(8)	4119.7(6)	3958.8(6)	3792.1(4)
GOF^a	1.01	–	–	–	1.08
R_{int}	0.0730	–	–	–	0.0790
χ^2	–	1.13	1.34	1.44	–
final R indices					
$[I > 2\sigma(I)]$ $R1^c/wR2^d$	0.0714/0.1855				0.0652/0.1786
all data $R1^c/wR2^d$	0.1154/0.2043				0.1024/0.1924

$^a S = [\sum w(F_0^2 - F_c^2)^2/(N_{obs} - N_{param})]^{1/2}$. $^b I > 3\sigma(I)$ (**1-Gd**). $^c R1 = \sum ||F_0| - |F_c||/\sum |F_0|$. $^d wR2 = [\sum w(F_0^2 - F_c^2)^2/\sum wF_0^2]^{1/2}$; $w = 1/[\sigma^2(F_0^2) + (aP)^2 + b]$ where $P = (\max(F_0^2,0) + 2F_c^2)/3$ with $a = 0.0628$ (**1-Sm**), 0.0684 (**1-Eu**), 0.1686 (**1-Tb**), 0.1185 (**1-Dy**), and 0.1025 (**1-Yb**); $b = 56.8404$ (**1-Sm**), 44.6121 (**1-Eu**), and 42.5345 (**1-Tb**). $^e w = 1/[\sigma^2(|F_0|) + (0.0001F_0)^2]$ and $P = \sum w(|F_c| - |F_0|)^2$ (**1-Gd**).

involving a wide variety of metal cations, anions, organic ligands, and solvents.[20] To date, there have been four mechanisms proposed to explain the *in situ* formation of oxalate: (1) the reductive coupling of dissolved carbon dioxide,[21] (2) the oxidation of ethanol or oxidative coupling of methanol using nitrate as oxidant,[22] (3) the decarboxylation of organic ligands, followed by reductive coupling of the resulting carbon dioxide,[23] and (4) the oxidation–hydrolysis in the presence of a metal catalyst implying the general decomposition of the organic ligand.[24] The carboxyl transfer observed for the pyrazine-2,5-dicarboxylate anion to render the isomer pyrazine-2,6-dicarboxylate during hydrothermal synthesis of $[Ln(2,5\text{-pzdc})_{0.5}(2,6\text{-pzdc})(H_2O)_3]$ compounds,[8b] following the Raecke process,[25] suggests that diazinedicarboxylato ligands can easily undergo a decarboxylative reaction upon heating. Cahill et al.[26] have elucidated that during the hydrothermal synthesis of the 2D $\{[Nd(2,3\text{-pzdc})(ox)\text{-}(H_2O)_2]\}_n$ (2,3-pzdc = pyrazine-2,3-dicarboxylato) the oxalato ligand results from the oxidation of the H_2pzdc through several intermediates by means of the ring-opening that occurs via cleavage of the C–N bond of the pyrazine ring followed by hydrolysis–oxidation of the resulting species (mechanism 4). The proposed mechanism also clarifies that prior to precipitation, the presence of metal cations, nitrogen-lone pairs, and carboxylate chelation likely accelerate the *in situ*

ligand formation and control end products; suggesting that the CO_2 liberated by decarboxylation does not participate in oxalate formation in contrast to what was previously reported.

The main conclusion of our study, in agreement with Cahill,[26] is that the pmdc decomposition reaction only takes place if the following three factors are met: relatively high temperature, oxygen containing atmosphere, and acidic pH. Performing the synthesis at room temperature, we obtain a novel family of oxalate-free **1-Ln** compounds. The crystallinity of this phase is highly depending on the pH value, obtaining crystalline products when the initial pH value of the reagent mixture is not modified (pH = 2.0–2.5). Additionally, the crystallinity is also improved when using a water/methanol mixture as solvent. At higher pH values, the great insolubility of **1-Ln** compounds leads to amorphous products. On the other hand, when the reaction takes place at higher temperatures (60–160 °C) and pH = 2.0–2.5 Ln/pmdc/ox compounds are obtained. A significant improvement of the crystallinity is achieved by pretreatment at 90 °C. This result suggests that the oxidation of pmdc takes place during the open-atmosphere pretreatment procedure, probably because of the dissolved molecular oxygen, and it requires a relatively high temperature in order to surpass the activation energy of the reaction. When the reaction temperature is set at 180–200 °C the oxalate-free **2-Ln** are obtained as low-crystalline products mixed with

Table 2. Crystallographic Data and Structure Refinement Details of Compounds 2-Ln

	2-La	2-Ce	2-Pr	2-Nd	2-Sm	2-Eu
empirical formula	$C_9H_6LaN_3O_{7.5}$	$C_9H_6CeN_3O_{7.5}$	$C_9H_6N_3O_{7.5}Pr$	$C_9H_6N_3NdO_{7.5}$	$C_9H_6N_3O_{7.5}Sm$	$C_9H_6EuN_3O_{7.5}$
formula weight	415.07	416.28	417.07	420.40	426.52	428.12
crystal system	monoclinic	monoclinic	monoclinic	monoclinic	monoclinic	monoclinic
superspace group	Pc	Pc	Pc	Pc	Pc	Pc
a (Å)	9.3759(2)	9.3148(2)	9.316(5)	9.445(3)	9.497(4)	9.543(3)
b (Å)	10.4558(2)	10.3964(2)	10.401(6)	10.424(4)	10.386(1)	10.348(4)
c (Å)	12.5447(2)	12.4509(3)	12.431(4)	12.504(2)	12.521(2)	12.551(3)
β (deg)	106.632(2)	106.685(3)	106.96(3)	107.11(6)	107.05(3)	107.16(3)
V (Å³)	1178.34(4)	1154.99(5)	1152.1(7)	1176.6(3)	1180.7(5)	1184.2(7)
GOF[a]	0.97	1.22	–	–	–	–
R_{int}	0.0264	0.0205	–	–	–	–
χ^2	–	–	1.38	2.15	1.34	1.73
final R indices						
$[I > 2\sigma(I)]$ R1[b]/wR2[c]	0.0268/0.0534	0.0220/0.0503				
all data R1[b]/wR2[c]	0.0353/0.0589	0.0232/0.0512				

	2-Gd	2-Tb	2-Dy	2-Ho	2-Er	2-Tm	2-Yb
empirical formula	$C_9H_6GdN_3O_{7.5}$	$C_9H_6N_3O_{7.5}Tb$	$C_9H_6DyN_3O_{7.5}$	$C_9H_6HoN_3O_{7.5}$	$C_9H_6ErN_3O_{7.5}$	$C_9H_6N_3O_{7.5}Tm$	$C_9H_6N_3O_{7.5}Yb$
formula weight	433.41	435.09	438.66	441.09	443.42	445.09	449.20
crystal system	monoclinic	monoclinic	monoclinic	monoclinic	monoclinic	monoclinic	monoclinic
superspace group	Pc	Pc	Pc	Pc	Pc	Pc	Pc
a (Å)	9.576(2)	9.553(5)	9.509(2)	9.448(5)	9.487(3)	9.389(8)	9.399(3)
b (Å)	10.321(2)	10.287(5)	10.356(4)	10.398(3)	10.432(3)	10.463(6)	10.455(5)
c (Å)	12.594(3)	12.636(3)	12.682(4)	12.624(4)	12.515(7)	12.427(3)	12.392(5)
β (deg)	107.25(3)	107.30(1)	107.38(3)	107.40(4)	107.25(2)	107.19(5)	107.05(2)
V (Å³)	1188.7(4)	1185.6(9)	1191.8(5)	1183.4(8)	1182.9(4)	1166.3(12)	1164.1(1)
χ^2	3.38	1.38	2.15	1.22	1.88	1.37	1.03

[a] $S = [\sum w(F_0^2 - F_c^2)^2/(N_{obs} - N_{param})]^{1/2}$. [b] $R1 = \sum||F_0| - |F_c||/\sum|F_0|$. [c] $wR2 = [\sum w(F_0^2 - F_c^2)^2/\sum wF_0^2]^{1/2}$; $w = 1/[\sigma^2(|F_0|) + (0.0004F_0)^2]$ and $P = \sum w(|F_c| - |F_0|)^2$.

previously mentioned Ln/pmdc/ox compounds. This behavior is attributed to an entropy driven effect that will be discussed in the following section. Shifting the pH to 5−6 or using an inert atmosphere slows down the pmdc ring-opening stage, bypasses the formation of Ln/pmdc/ox systems, and leads to crystalline **2-Ln** compounds. Thus, it can be concluded that the absence of oxygen and the nonacidic pH are crucial to obtain oxalate-free compounds.

Regarding the pmdc decomposition, it deserves to be noted that the ammonia molecules released after the ring-opening process[26] raise the pH value and inhibit a further decomposition, explaining why, when the initial pH is not modified, the Ln/pmdc/ox compounds are obtained instead of simple lanthanide oxalates.
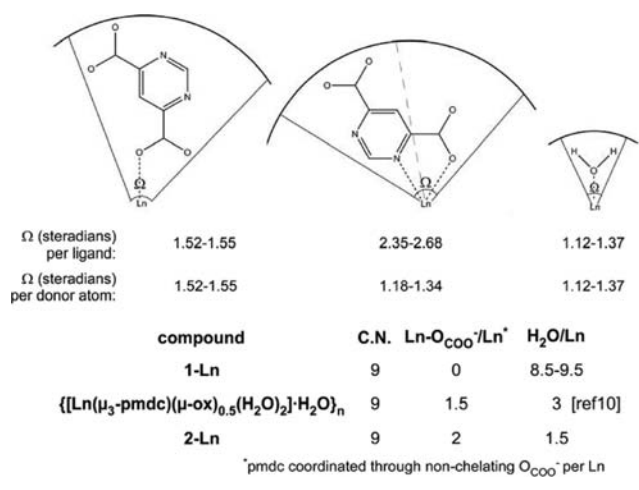
Synthetic Conditions: Dimensionality Control. The entropy driven desolvation pathway[27] that takes place at higher temperatures is known to favor the release of solvent molecules. This effect is clearly observed in the Ln/pmdc system, since the pmdc ligand raises its denticity to occupy the empty coordination positions, increasing the connectivity among the metal nodes. In any case, the temperature required for the formation of **2-Ln** increases on going forward in the lanthanide series, as it depends on the energetic penalty that must be paid because of the combined effect of the ligands steric hindrance and the ionic radius of the lanthanide.[28] In this sense, a study by means of the *Solid-G* program[29] revealed that the greater hindrance per occupied coordination position is due to the pmdc ligand coordinated by its nonchelating oxygen atom (Scheme 2), a coordination mode that is only present in compounds **2-Ln**. Therefore, the smaller the lanthanide ion the greater the steric hindrance and the higher the required

temperature to obtain **2-Ln**. This fact is reinforced by the increase of the hydration energy on going forward in the lanthanide series that hinders the release of the coordinated water molecules. On the other hand, the formation of **2-Ln** compounds in synthetic conditions in which oxalate anions are present is explained taking into account the lower H_2O/Ln ratio present in **2-Ln** in comparison with those of the Ln/pmdc/ox phases. Therefore, the entropy driven desolvation reaction favors the formation of **2-Ln** at higher temperatures ($T > 180$ °C).

To get further detail on the structural trends of the Ln/pmdc system, the effect of the synthesis temperature was assessed for selected lanthanides where the LnX_3/pmdc/H_2O (X = NO_3^- or Cl^-) molar ratio was fixed at 1:2:18518 (Scheme 3). The solutions were prepared by bubbling N_2 gas, and a pH value of 5.5 was adjusted. In general, the formation of compounds **1-Ln** occurs at room temperature while compounds **2-Ln** are obtained above 180 °C. However, when applying intermediate temperatures, four new oxalate-free Ln/pmdc compounds (named **A**, **B**, **C**, and **D**) were obtained (Supporting Information).

In view of these results, it becomes evident again that the entropic effect with increasing temperature stabilizes more compact frameworks in which the H_2O/Ln ratio experiences a progressive decrease as the coordinated water molecules are replaced by nonchelating O_{COO^-} atoms, which implies an increase of the connectivity. Compounds **A−D** present a general formula of $[Ln(pmdc)_{1.5}(H_2O)_y]\cdot xH_2O$ ($y = 1−2.5$), with a coordination water content that is between that of compounds **1-Ln** and **2-Ln**. This feature suggests that the crystal structures of these new compounds are probably
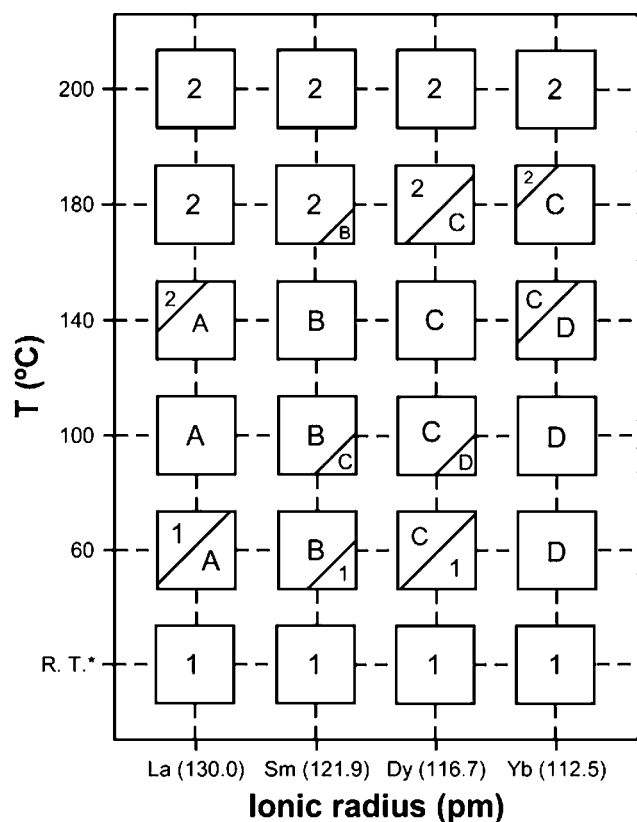
Scheme 1. Synthetic Conditions on the Ln/pmdc System
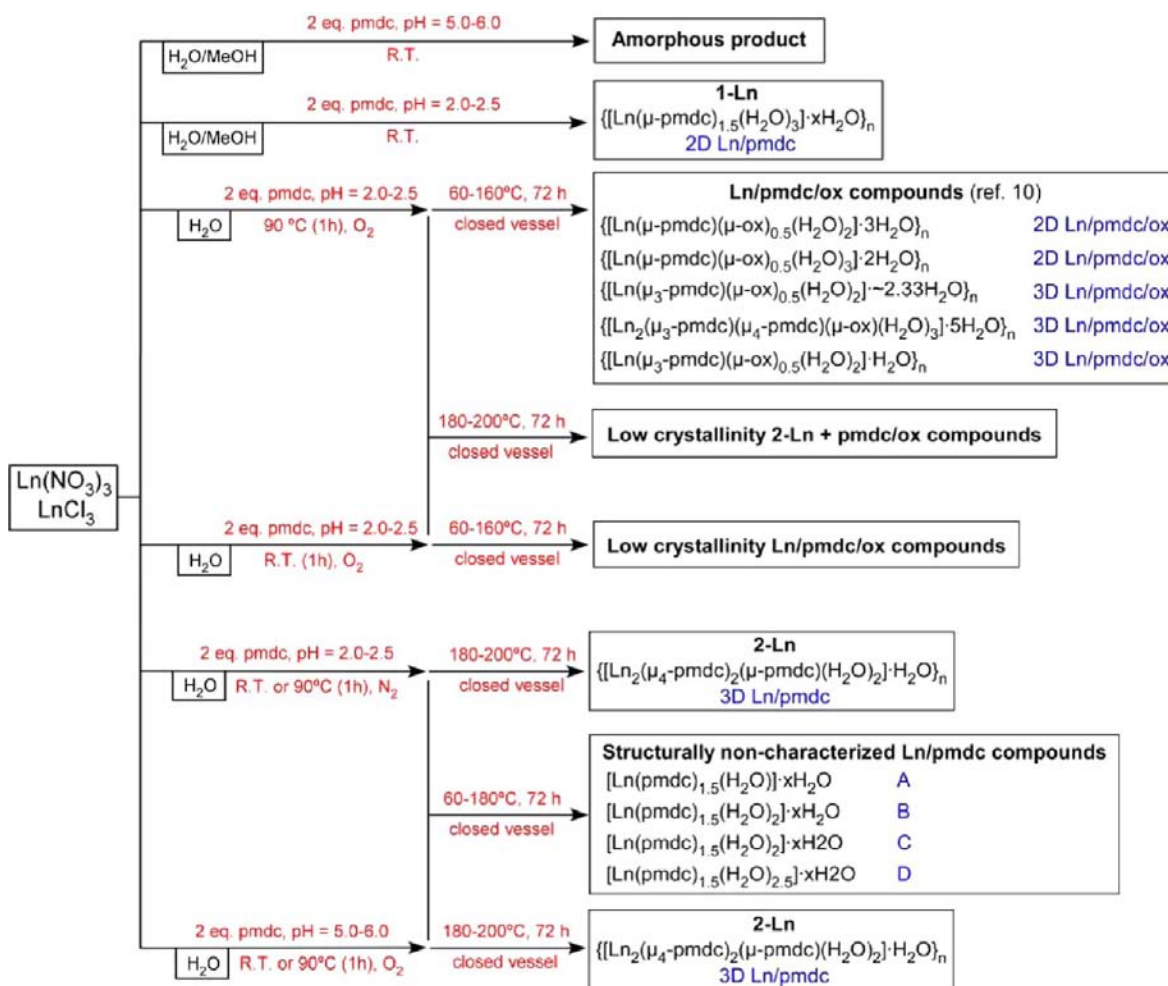
Scheme 2. Solid Angle (Ω) Occupied by Each Ligand around the Metal Center, Together with Some Relevant Parameters of the Compounds

| Ω (steradians) per ligand: | 1.52-1.55 | 2.35-2.68 | 1.12-1.37 |
| Ω (steradians) per donor atom: | 1.52-1.55 | 1.18-1.34 | 1.12-1.37 |

compound	C.N.	Ln-O_{COO^-}/Ln*	H_2O/Ln
1-Ln	9	0	8.5-9.5
$\{[Ln(\mu_3\text{-pmdc})(\mu\text{-ox})_{0.5}(H_2O)_2]\cdot H_2O\}_n$	9	1.5	3 [ref10]
2-Ln	9	2	1.5

*pmdc coordinated through non-chelating O_{COO^-} per Ln

midway between the 2D (**1-Ln**) and the compact 3D (**2-Ln**) structures. All these results confirm not only the coordinative capability and versatility of the pmdc ligand in constructing a wide variety of crystal structures but also the specific synthetic conditions that prevent oxalate formation.

Crystal Structure of 1-Ln. The crystal structure of these compounds consists of the stacking of neutral [Ln(μ-pmdc)$_{1.5}$(H$_2$O)$_3$] layers that accommodates crystallization water molecules in between. In the layers, the crystallographically independent metal centers, Ln1 and Ln2, are surrounded by a N$_3$O$_3$Ow$_3$ donor set (Figure 2), with a geometry close to a tricapped trigonal prism as revealed the continuous shape measurements (CShM).[30] The S(ttp) results [0.88 (Yb) and 1.23 (Sm)] show that the less the ionic radius of the lanthanide(III) atom, the less distortion with regard to the ideal shape. The coordination Ln−N and Ln−O bond lengths and angles are within the range observed for analogous carboxylic azine ligands.[31]

Each metal center coordinates to three almost planar bis-bidentate pmdc ligands by means of five member chelate rings, while three coordinated water molecules complete the coordination sphere. These Ln(μ-pmdc)$_3$(H$_2$O)$_3$ units are joined to one another (Ln⋯Ln distances of *ca.* 7.2 Å), generating layers of hexagonal six-membered rings (Ln⋯Ln⋯Ln, ranging from 112.4 to 123.9°) that comprise a honeycomb pattern. This fact forces the pmdc ligands to arrange outward the mean plane of the layer established by the metal centers (47.8° for pmdc1, 15.6° for pmdc2, and 52.28° for pmdc3), leaving the carboxylate oxygen atoms exposed to the interlayer space ready to interact with the solvent molecules. The topological analysis performed by the *TOPOS* program package,[32] as can be seen in Figure 3, indicates an

Scheme 3. Plot of Temperature vs. Ionic Radius on the Ln(III)/pmdc System[a]

Figure 3. 2D topological network showing the six-membered rings.

[a]The room temperature (*) tests have been performed with continuous stirring and without hydrothermal conditions.

uninodal two-dimensional **hcb** topological network (3-c net), the point symbol being (6^3).

The piling up of the layers takes place along the c axis in an ABA fashion creating intricate channels that are filled by the crystallization water molecules, which account for the 34% of

the unit cell volume (Figure 4).[33] The hydrogen bonding interactions established among them generate water clusters in the form of isolated R7 rings[34] anchored to the walls of the Ln-pmdc framework by means of an extensive network of hydrogen bonds.

It is worth noting that compound **1-Gd** undergoes a phase transition toward a modulated commensurate structure with a
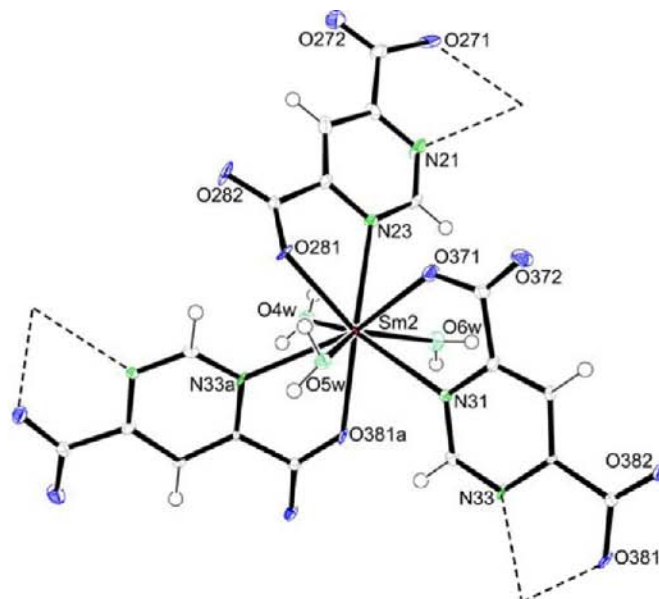

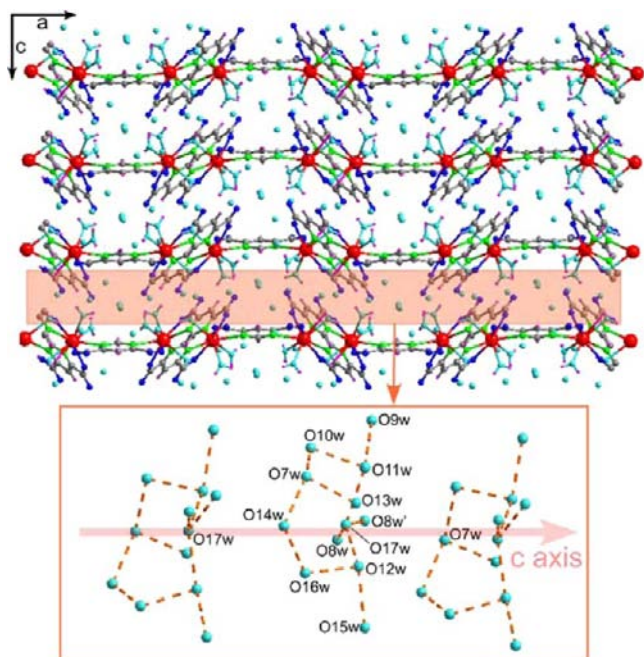**Figure 2.** Coordination environments of the Sm1 and Sm2 atoms in compound **1-Sm**.

Figure 4. Packing of compound **1-Sm** showing the chains of solvent molecules.
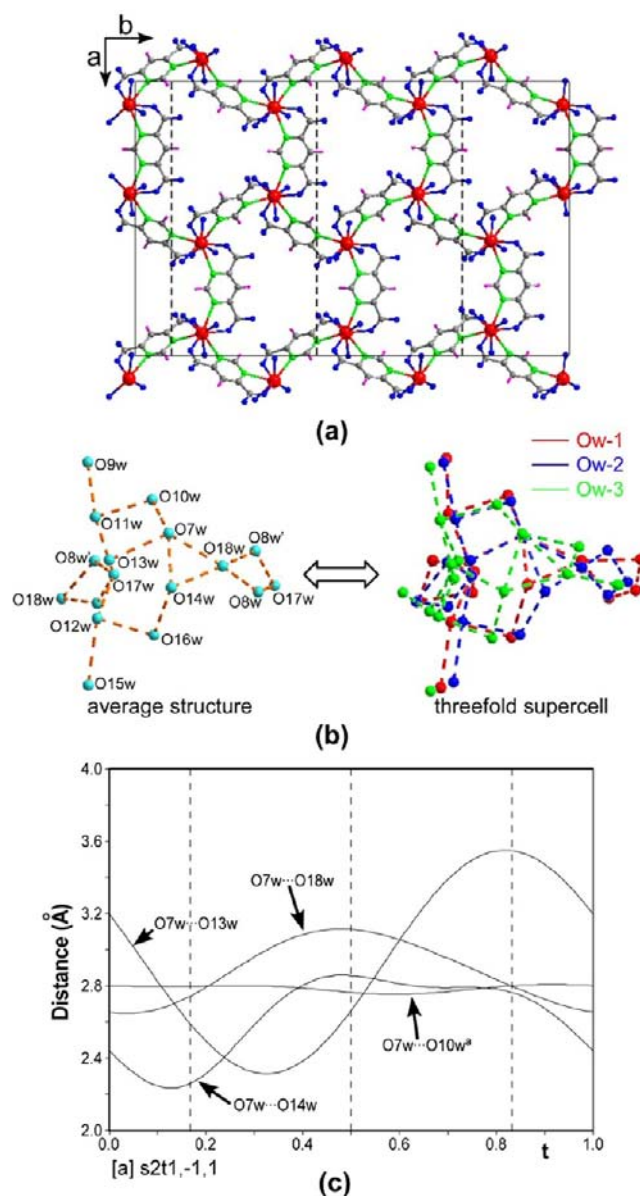

(a)

(b)

(c)

Figure 5. (a) 3-fold supercell of compound **1-Gd** (crystallization water molecules have been omitted). (b) Distortions in the hydrogen bonded clusters of the supercell vs the average structure. (c) t-plot showing variations in the hydrogen bonding distances.

commensurate **q** vector ($\mathbf{q} = 0\ ^1/_3\ 0$) in the superspace group $P2_1/c(0\backslash\beta0)s0$ upon cooling down to 100 K. The super-structure consists of all the atoms of the asymmetric unit but triply split in agreement with the 3-fold supercell. The atoms belonging to the $[\mathrm{Gd}(\mu\text{-pmdc})_{1.5}(\mathrm{H_2O})_3]$ layers are hardly affected by the modulation, but the crystallization water molecules move more sharply introducing remarkable distortions into the hydrogen bonding clusters. This effect becomes clear when overlapping the hydrogen bonded rings of the three superstructure positions in the vicinity of the O7w atom. The *t*-plot carried out for the hydrogen bonding distances involving the neighboring atoms of O7w leads to the same conclusion. In fact, an additional O18w water molecule has been included to complete the hydrogen bonding scheme, which allows the water rings to be joined together and thus lead to T7(0)A2 chains (Figure 5). These subtle variations found for the geometry of the water clusters in the commensurate structure, compared with the periodic struc-tures, give some insights about how modulation proceeds throughout the crystal.

Thermal studies of compound **1-Gd** reveal that some of the crystallization water molecules are lost spontaneously when removing the compound from the mother liquors, as its release starts from room temperature up to 340 °C, to render a $\mathrm{Gd_2O_3}$ residue above 650 °C (Supporting Information). The XRPD profiles of this compound show a rapid crystallinity decrease above 30 °C due to the release of the crystallization water molecules. The final anhydrous product at 150 °C is amorphous.

Crystal Structure of 2-Ln. The crystal structure of compounds **2-Ln** consists of a 3D neutral open framework built up from the junction of the Ln(III)−pmdc layers found in compounds **1-Ln** where two of the coordinated water molecules of both Ln1 and Ln2 atoms have been replaced by the noncoordinated carboxylate oxygen atoms from the pmdc ligands (Figure 6). As a result, the Ln(III) centers are surrounded by a $\mathrm{N_3O_5Ow}$ donor set that severely increases

the distortion of the coordination polyhedra with regard to the ideal shapes (jgsp and ttp), as indicated by the CShM [S(jgsp) = 2.35−2.14 and S(ttp) = 3.29−3.10, for **2-La** and **2-Ce**, respectively].

The coordination of two additional hexadentate μ_4-$\kappa^2\mathrm{N,O}{:}\kappa^2\mathrm{N',O'}{:}\kappa\mathrm{O''}{:}\kappa\mathrm{O'''}$−pmdc ligands to the Ln(III) centers imposes shorter Ln⋯Ln distances than those found through the bis-bidentate bridge (mean values: 6.6 vs 7.3 Å). As a consequence, the three chelating pmdc are forced to be more twisted (dihedral angles: 40.5−56.0° for **2-Ce** vs 45.8−78.0° for **1-Ln**), exerting a remarkable distortion inside the six-membered rings (Figure 7). The interlayer coordination of the O272 atoms to the Ce2 atoms is also responsible for these distortions, which become more evident when focusing the junction among the rings, since they are tilted 63.3°. As a result, the layers are no longer flat, as it can be derived from the mean deviance of the Ln(III) atoms from the mean plane of the ring
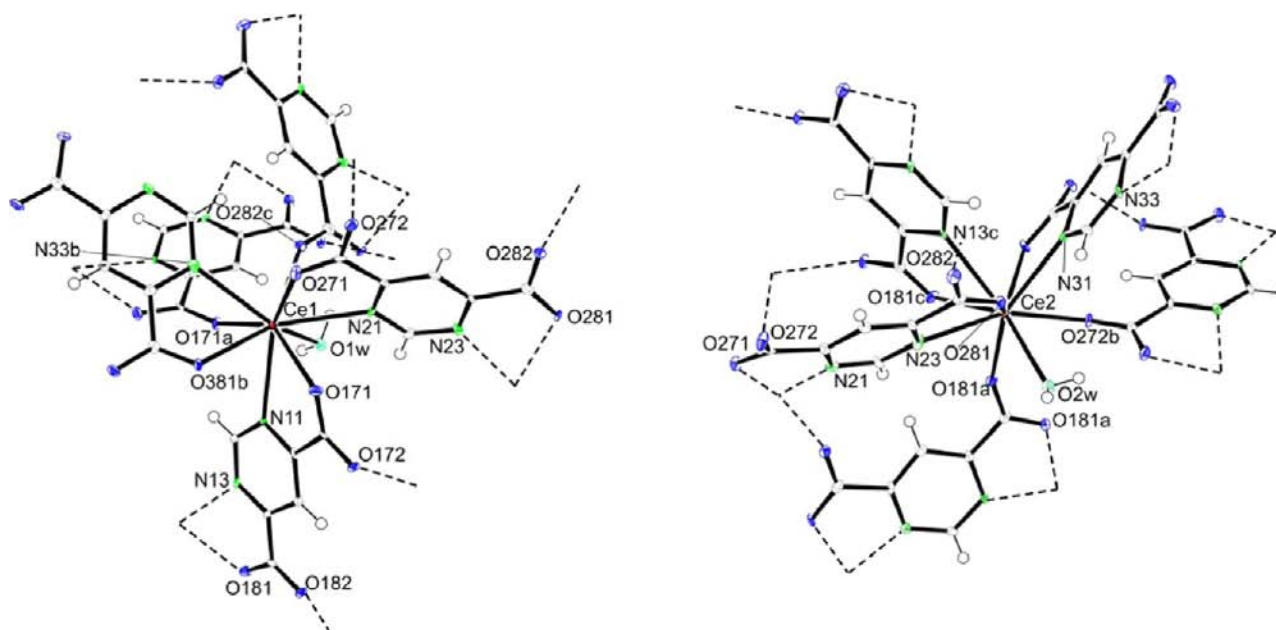
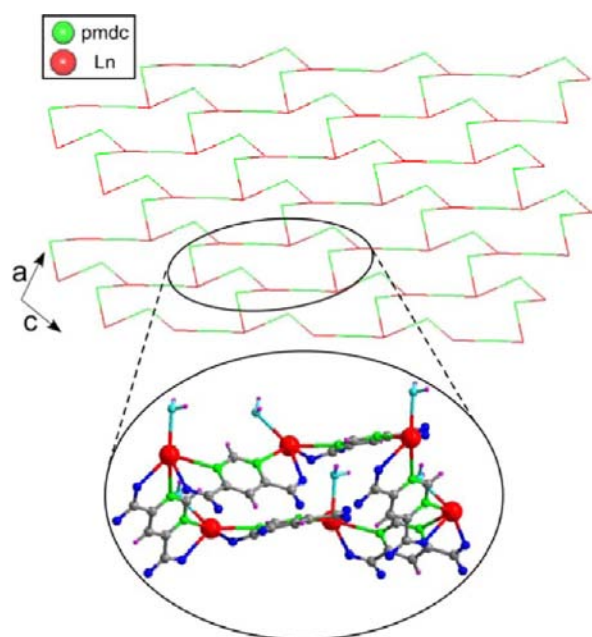**Figure 6.** Coordination environments of the Ce1 and Ce2 atoms in compound **2-Ce**.

Figure 7. Distorted six-membered rings that form the herringbone pattern in **2-Ce**.

Figure 8. Building up of the 3D framework by the coordination of the nonchelating oxygen atoms.

and they resemble a herringbone pattern. The piling up of the corrugated layers takes place along the crystallographic *b* axis where the nonchelating carboxylate oxygen atoms (O182, O272, and O282) of the hexadentate pmdc ligands serve as a junction between layers by coordinating to the metal centers belonging to the adjacent layers, leading to the overall 3D open framework (Figure 8). The crystallization water molecule is sited in a small isolated cavity of the compact building. The sharp rise of the connectivity provides a (4,4,5,5-c) network that possesses a new topology that has been named as **jcr2**, the point symbol being $(3.4.5^2.6^2)(3.4.5^2.6^4.7^2)(3.4.5^2.6^4.8^2)$-$(4.5.6^3.8)$.

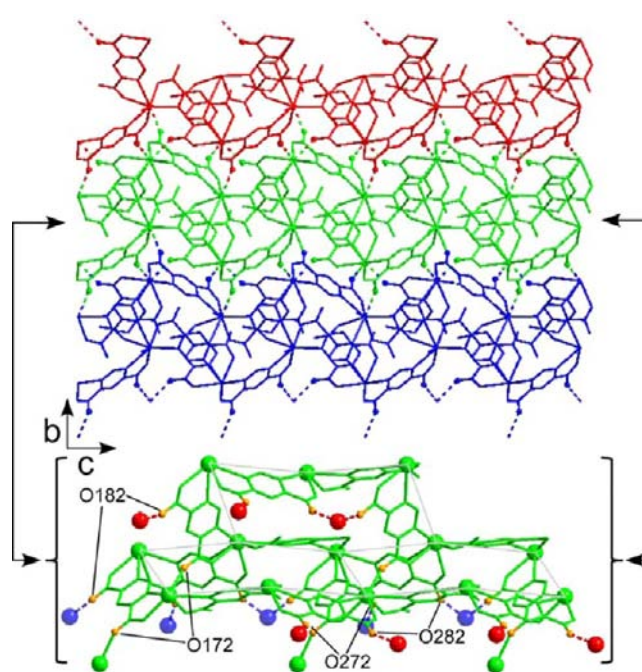The thermal analysis performed over compound **2-Pr** shows a first endothermic process between 50 and 120 °C, which corresponds to the release of the crystallization water molecules. The loss of the solvent does not promote any significant structural change until 190 °C, where the loss of the coordination water molecules takes place. The anhydrous compound remains stable up to 390 °C, temperature at which the oxidation of the pmdc ligand occurs to lead to PrO_2 as final product at 550 °C.

FTIR Analyses of the Ln/pmdc System. An exhaustive analysis of the IR spectra of compounds **1-Ln** and **2-Ln** has let us to accurately assign all bands (Figure 9), allowing us to distinguish between the two different coordination modes of the pmdc ligand; unlike what happened for the compounds of the previously published Ln/pmdc/ox system in which the
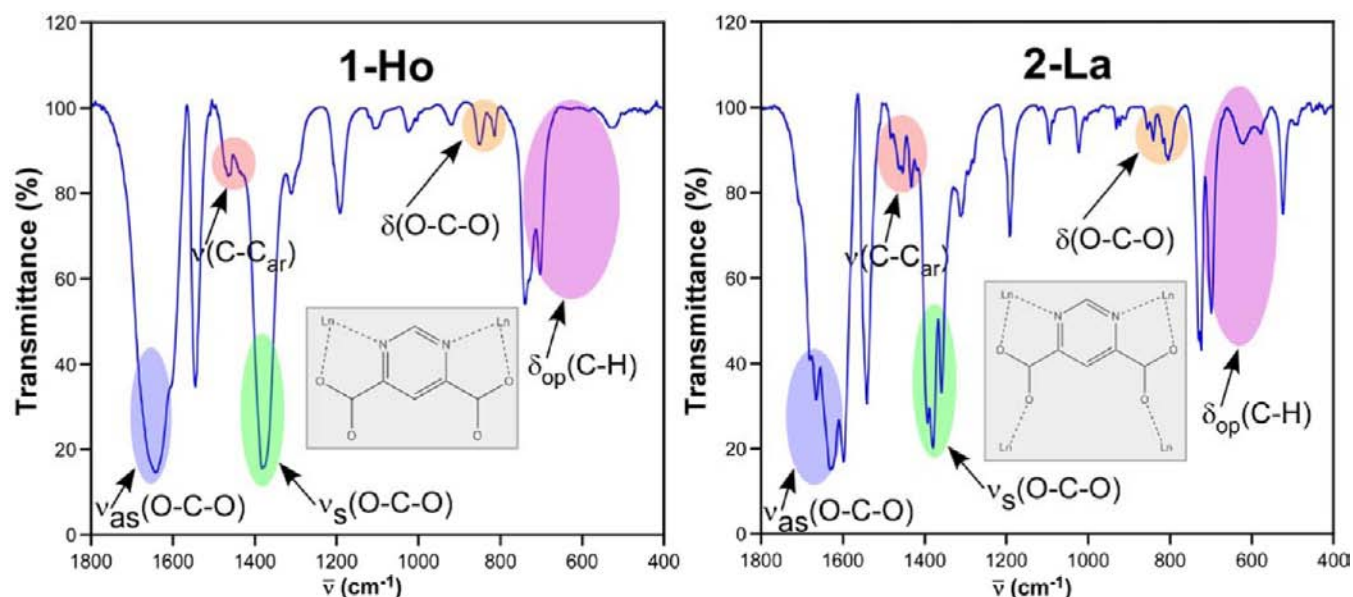
Figure 9. IR spectra for compounds **1-Ho** and **2-La** showing the most characteristic differences.

oxalato and pmdc ligands are overlapping.[10] All spectra share the presence of broad and intense bands in frequency region of 3550−3200 cm⁻¹, assigned to the characteristic peaks of OH vibration of free water; the intense vibrations around 1650 cm⁻¹ and 1360 cm⁻¹ correspond to the asymmetric and symmetric stretching vibrations of the carboxylate groups, while at lower frequencies, the remaining bands are attributed to the distortions originated in the aromatic ring of the pmdc ligand. However, compounds **2-Ln** exhibit a greater number of bands derived from the simultaneous presence of the bis-chelating μ-κ^2N,O:κ^2N′,O′ and the hexadentate μ_4-κ^2N,O:κ^2N′,O′:κO″:κO‴ coordination modes. In particular, a strong splitting is observed in the asymmetric O−C−O stretching into three other bands that appear at higher wavenumbers, just as in its symmetric stretching and its outward ring plane displacement, where the relative intensity between the major bands is altered. The change in the coordination also affects the vibrational modes of the aromatic ring, as it goes from two to four the number of observable bands around 1460 cm⁻¹, while the intensity of the displacement of the aromatic hydrogen atoms outward the ring plane increases notoriously.

All these observations help us in analyzing the non-structurally characterized **A**, **B**, **C**, and **D** compounds. As shown in Supporting Information, compound **A** exhibits a strong splitting in the asymmetric and symmetric O−C−O vibrations, indicative of the presence of both the bis-bidentate and hexadentate modes; whereas this splitting does not exist in compound **D**, with almost the same bands of **1-Ln** compounds. The IR spectra of **B** and **C** compounds are representative of an intermediate situation, where the splitting is perceptible but weaker than that of **A** compound. These results are in good agreement with the trend found for the effect of the temperature induced entropy driven desolvation process and the lanthanide contraction that takes place along the series (Scheme 3). Once again, a larger ionic radius favors the presence of sterically more hindered coordination modes and higher temperatures are required for these modes to be present for shorter ionic radii.

Magnetic Properties. The temperature-dependent magnetic susceptibility data of compounds **1-Ln** and **2-Ln**, with the

exception of the lanthanum compounds, have been measured. The room temperature $\chi_M T$ values are close to those expected for the ground states derived from their strong spin−orbit coupling. The lanthanide(III) atoms can be classified into three different groups according to their magnetic behavior. The group consisting of Ce, Pr, Nd, Tb, Dy, Ho, Er, Tm, and Yb stands out by the progressive decrease in the $\chi_M T$ product as lowering the temperature derived from both a selective depopulation of the excited Stark levels and antiferromagnetic interaction between lanthanide ions. To obtain a rough quantitative estimation of the magnetic interaction, an expression for the χ_M can be defined by assuming a splitting of the m_j energy levels ($H = \Delta J z^2$) in an axial crystal field.[35] It must be noted, the energy separation of Sm(III) and Eu(III) ions between the ground state and the first excited state is so small that the first excited state may be thermally populated and has to be therefore evaluated in the expressions of the magnetic susceptibility.[36] The Gd(III) ions are exceptions among the lanthanide series because their ⁸S₇/₂ ground state allows to analyze quantitatively their magnetic interactions by applying a spin-only Hamiltonian. Plots of χ_M^{-1} vs T for the gadolinium compounds (Supporting Information) obey the Curie−Weiss law, giving $C = 8.25(2)$ cm³ K mol⁻¹, $\theta = -0.11(2)$ K and $C = 13.35(1)$ cm³ K mol⁻¹, $\theta = -1.32(2)$ K for compounds **1-Gd** and **2-Gd**, respectively. Taking into account the 2D crystal structure of compound **1-Gd**, the magnetic data was analyzed in the whole temperature range (5−300 K) using the expression derived by Curély[37] with S = ⁷/₂ (eq 1).

$$\chi_{Gd} = \frac{Ng^2\beta^2}{3kT} \frac{S(S+1)(W_1 + W_2)}{(1-u^2)^2} \tag{1}$$

In the expression, $u = \coth[JS(S+1)/kT] - kT/JS(S+1)$, $W_1 = (1+u^2)^2 + 4u^2$, $W_2 = 4u(1+u^2)$, J is the exchange coupling parameter between adjacent spins through the pmdc bridge, and all of the other parameters have their usual meanings. The absence of an appropriate expression that considers the magnetic interaction in the 3D framework has prevented us to evaluate its magnitude in compound **2-Gd**. However, the obtained θ value indicates the greater antiferromagnetic

character of the latter, although still being almost negligible, in good agreement with the presence of a shorter second exchange pathway through the nonchelating oxygen atoms of the pmdc. The χ_M expressions derived for all the lanthanide-(III) atoms can be found in the Supporting Information. The best fitting results, for the 50−300 K temperature range (5−300 K for compound **1-Gd**), are gathered in Table 3. Figure 10

Table 3. Best Least-Squares Fits of the Magnetic Data[a]

compd	g	Δ (cm^{-1})
1-Nd	0.71	2.20
1-Tb	1.47	0.18
1-Dy	1.30	0.11
1-Ho	1.23	0.29
1-Er	1.23	0.40
1-Tm	1.13	0.31
1-Yb	1.12	3.32
2-Ce	0.86	5.18
2-Pr	0.76	3.26
2-Nd	0.73	2.04
2-Tb	1.47	0.21
2-Dy	1.26	0.12
2-Ho	1.23	0.25
2-Er	1.23	0.38
2-Tm	1.13	0.33
2-Yb	1.12	3.34
compd	g	λ (cm^{-1})
1-Sm	0.28	225.39
1-Eu	5.00	373.57
2-Sm	0.29	229.74
2-Eu	5.01	362.17
compd	g	J (cm^{-1})/θ (K)
1-Gd	2.02	−0.01/−0.11
2-Gd	2.01	−/−1.32

[a] Δ is the zero-field splitting parameter, and λ is the spin−orbit coupling parameter.

Figure 10. $\chi_M T$ (o) vs T plot showing the best theoretical fit (−) for compounds **1-Gd**, **2-Ce**, and **1-Sm**.

shows the best fitting curve of the $\chi_M T$ product for three selected compounds. The results show that the magnetic interaction is almost negligible among the Ln(III) ions.

Luminescence Properties. Lanthanide compounds are known for their photoluminescent properties, as they have been used to develop several technological applications that encompass not only fluorescent tubes and color televisions but also immunoassays,[38] optical amplifiers,[39] and in future perhaps metal−organic light-emitting diodes.[40] The solid state photoluminescence spectra of compounds **1-Nd**, **1-Eu**, **1-Tb**, **2-Nd**, **2-Eu**, and **2-Tb** were recorded at room temperature, and the characteristic emission bands for the corresponding Ln(III) ions are shown in Figure 11.

The neodymium compounds **1-Nd** and **2-Nd** display an emission band at 1061 nm ($^4F_{3/2} \rightarrow {}^4I_{11/2}$) and another one at 1332 nm ($^4F_{3/2} \rightarrow {}^4I_{13/2}$) in the NIR region under excitation at 800 nm in the $^4F_{5/2}$ level. The first band, which is potentially applicable to laser emission, fluoroimmunoassays, and in vivo detection,[41] is dominant in both cases. Upon excitation at 355 nm, compounds **1-Eu** and **2-Eu** display intense red luminescence with five bands occurring at 580, 590, 615, 665, and 690 nm that can be assigned to $^5D_0 \rightarrow {}^7F_J$ transitions ($J = 0, 1, 2, 3,$ and 4, respectively).[42] The $^5D_0 \rightarrow {}^7F_2$ and $^5D_0 \rightarrow {}^7F_1$ transitions are ED and MD, respectively, which makes the former (known as hypersensitivity) to be extremely sensitive to
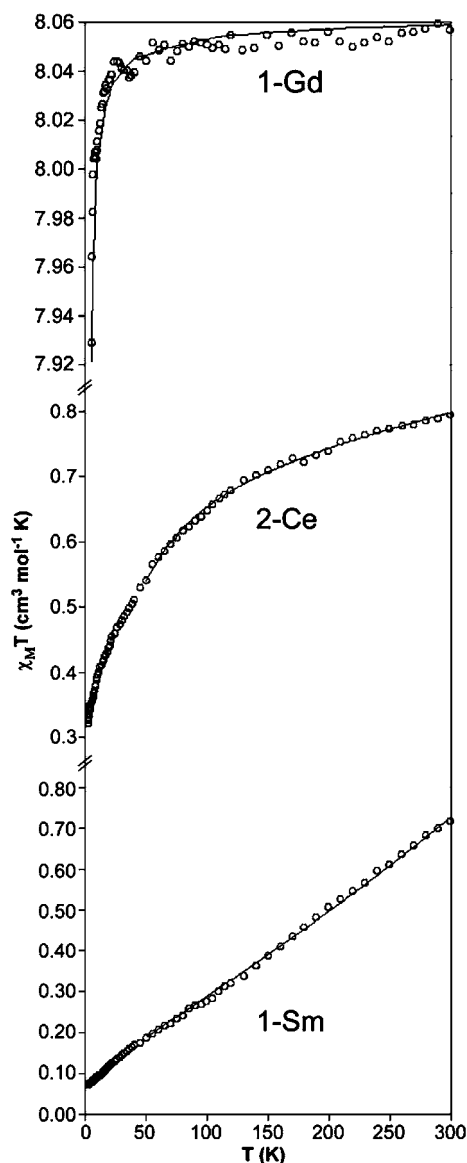
site symmetry, whereas the latter is mainly sensitive to the magnetic dipole effect created by the crystal field environment and is practically not influenced by the chemical surroundings of the ion. The intensity of the $^5D_0 \rightarrow {}^7F_2$ transition, which is responsible for brilliant red emission of these compounds, is about 5 times stronger than that of the $^5D_0 \rightarrow {}^7F_1$ band in both cases, indicating that the Eu^{3+} ions occupy low-symmetry sites without inversion center in agreement with the structural analyses. Moreover, the presence of the weak symmetry-forbidden $^5D_0 \rightarrow {}^7F_0$ transition at 577 nm, which is induced by crystal field J mixing, is allowed on non-inversion sites. The $^5D_0 \rightarrow {}^7F_3$ transition is very weak according to its forbidden character (both in magnetic and induced electric dipole schemes). Regarding the terbium compounds, both of them emit green luminescence upon excitation at 355 nm with the bands peaking at 490, 540, 580, 620, and 650 nm. These are originated from the characteristic $^5D_4 \rightarrow {}^7F_J$ transitions ($J = 6, 5, 4, 3,$ and 2). As expected, in higher Tb^{3+} concentrated systems, although the 355 nm excitation light populates level $^5D_3$ the observed emission corresponds to $^5D_4$ level being the
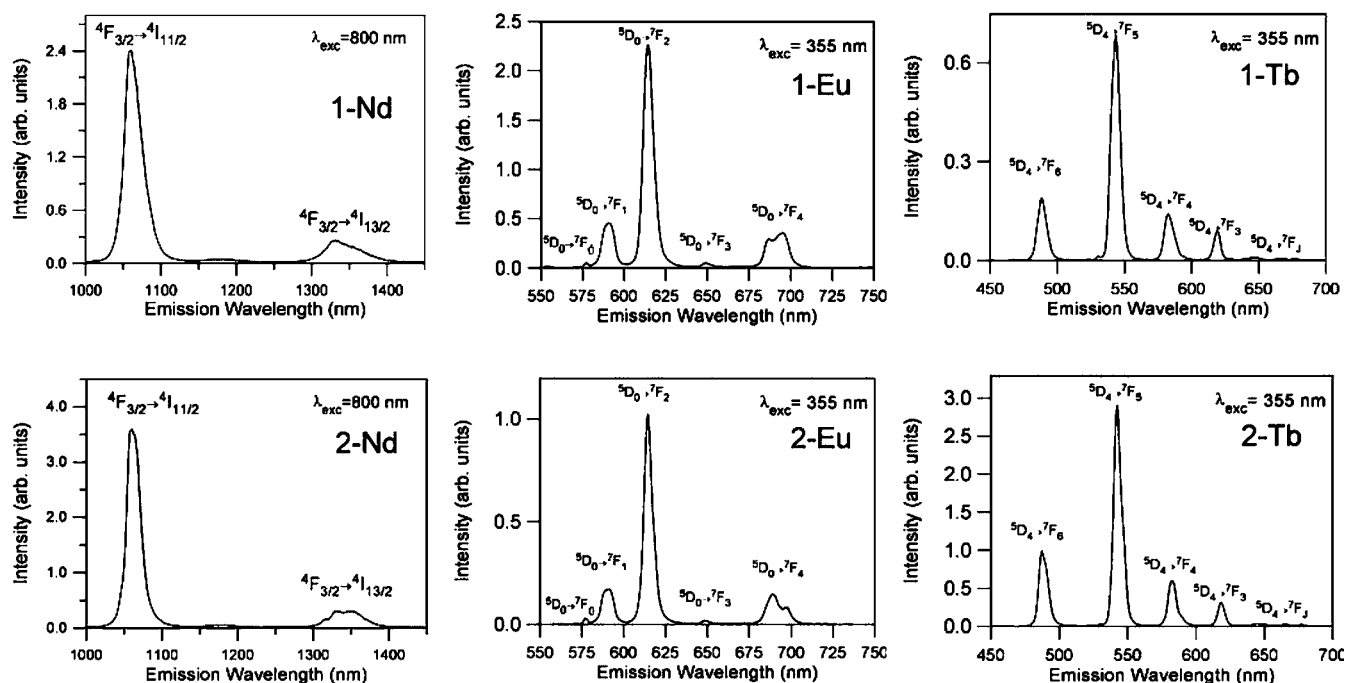
Figure 11. Room temperature emission spectra obtained under excitation at 800 nm for **1-Nd** and **2-Nd**; and at 355 nm for compounds **1-Eu**, **2-Eu**, **1-Tb**, and **2-Tb**. The emissions around 650 nm in compounds **1-Tb** and **2-Tb** correspond to transitions $^5D_4 \rightarrow {}^7F_J$ ($J = 0, 1, 2$).

intensity of the $^5D_4 \rightarrow {}^7F_5$ transition the strongest one.[42] This transition has the largest probability for both electric-dipole and magnetic-dipole induced transitions.[43]

The measurement of the experimental emission decay curves from the $^4F_{3/2}$ (Nd³⁺), $^5D_0$ (Eu³⁺), and $^5D_4$ (Tb³⁺), excited states for all compounds allowed us to effectively estimate the lifetimes in each case (Table 4). The decay curves are shown in

Table 4. Lifetime Values of Compounds

compd	τ (μs)	compd	τ (μs)
1-Nd	19	**2-Nd**	22
1-Eu	290	**2-Eu**	391
1-Tb	593[a]	**2-Tb**	783

[a]This value corresponds to $\langle \tau \rangle$.

the Supporting Information and can be fitted to a single-exponential function, to a good approximation, except for compound **1-Tb**. The decay curve in this case can be fitted to a double-exponential function, $[I = A + A_1 \exp(-t/\tau_1) + A_2 \exp(-t/\tau_2)$, where τ_1 and τ_2 are the fast and slow components of the luminescent lifetimes and A, A_1, and A_2 are the fitting parameters]. In this case, an average lifetime can be defined as $\langle \tau \rangle = A_1\tau_1^2 + A_2\tau_2^2/A_1\tau_1 + A_2\tau_2$; however, in order to reduce the fitting errors in the calculation of the average lifetime for this sample, we have used in Table 4 the average lifetime defined by the equivalent expression $\langle \tau \rangle = (\int tI(t)\mathrm{d}t)/(\int I(t)\mathrm{d}t)$.

In light of these results, a significant increase of the lifetimes of compounds **2-Ln** in comparison with those of compounds **1-Ln** can be inferred. There are several alternative deactivation pathways of the excited state of a lanthanide(III) center in the form of nonradiative processes, such as the back-energy transfer to the sensitizer,[44] electron transfer quenching,[44c,45] and most importantly, quenching by matrix vibrations. In particular, the O−H oscillators are very effective quenchers of luminescence,[46] explaining the observed increase in the lifetime according to the

decrease of coordination water molecules present in the chromophores of compounds **2-Ln**. Concerning the emission efficiency of the Ln(III) center, which decreases in the relative order Tb(III) > Eu(III) > Nd(III), this behavior can be understood by taking into account that the extent of excited state deactivation by O−H vibronic coupling from water molecules is inversely proportional to the energy gap between the emitting state and the ground state manifold.[47] This energy gap is approximately 5200 cm⁻¹ for Nd³⁺ ($^4F_{3/2} \rightarrow {}^4I_{15/2}$), 12200 cm⁻¹ for Eu³⁺ ($^5D_0 \rightarrow {}^7F_6$), and 14800 cm⁻¹ for Tb³⁺ ($^5D_4 \rightarrow {}^7F_0$), so that an efficient coupling of the Nd³⁺ excited state occurs. For Eu³⁺ excited states the coupling is to the third vibrational overtone of proximate OH oscillators ($\nu_{OH} \sim$ 3300−3500 cm⁻¹), and to the fourth harmonic in the case of Tb³⁺, consistent with the observed less efficient quenching because the Franck−Condon overlap factor is less favorable.

■ CONCLUSIONS

In the present work, the crystal structures of two families of lanthanide/pyrimidine-4,6-dicarboxylate compounds are reported, both of which are built up from the recurrent bisbidentate coordination mode of the pmdc ligand. It is well-known that the N-heteroaromatic-carboxylate ligands generate oxalate through its partial decomposition in the presence of lanthanides, so the success in obtaining these oxalate-free compounds requires a rigorous control over the synthetic conditions. The exhaustive study carried out to check the influence of the reaction temperature, pH, atmosphere, and the lanthanide ionic size has enabled us to access to a wide unexplored diversity of Ln/pmdc compounds, showing not only the validity of the method but also that the entropy driven desolvation pathway is fulfilled. The distorted honeycomb layers found in compounds **1-Ln** are packed generating interlamellar voids occupied by highly flexible crystallization water molecules aggregates, which are responsible for the modulation found for the low temperature phase of the **1-Gd**

compound. The replacement of two of the three coordination water molecules by two μ_4-κ^2N,O:κ^2N′,O′:κO″:κO‴−pmdc ligands in the chromophores of compounds **2-Ln** allow the layers to be joined together, rendering a compact 3D framework with the new topology **jcr2**. The variability of the coordination modes of the pmdc, including that of the nonstructurally characterized **A−D** compounds, has been monitored by the FTIR spectroscopy.

The magnetic behavior of the compounds is dominated by the spin−orbit coupling and the ligand field perturbation with an almost negligible contribution of the exchange coupling between the lanthanide atoms that is practically independent of the coordination mode. Luminescence measurements performed over the neodymium, europium, and terbium compounds show the characteristic near-IR, red, and green emissions, respectively. Furthermore, the lifetimes of these compounds estimated from the experimental emission decay curves from the excited states show a marked increase for compounds **2-Ln** compared to **1-Ln**, which is attributed to the decrease of coordination water molecules present in the chromophores of the former as they are replaced by carboxylic oxygen atoms of the pmdc ligands.

■ ASSOCIATED CONTENT

Ⓢ Supporting Information

Elemental analyses, IR data, X-ray analysis, thermogravimetric measurements, magnetic susceptibility data, emission decay curves, and cif files. This material is available free of charge via the Internet at http://pubs.acs.org.

■ AUTHOR INFORMATION

Corresponding Author

*Email: oscar.castillo@ehu.es, javier.cepeda@ehu.es. Fax: +34-94601-3500.

Notes

The authors declare no competing financial interest.

■ ACKNOWLEDGMENTS

■ REFERENCES

(1) (a) Kitagawa, S.; Kondo, M. *Bull. Chem. Soc. Jpn.* **1998**, *71*, 1739. (b) Batten, S. R.; Robson, R. *Angew. Chem., Int. Ed.* **1998**, *37*, 1460. (c) Blake, A. J.; Champness, N. R.; Hubberstey, P.; Li, W. S.; Withersby, M. A.; Schröder, M. *Coord. Chem. Rev.* **1999**, *183*, 117. (d) Moulton, B.; Zaworotko, M. *Chem. Rev.* **2001**, *101*, 1629. (e) Moulton, B.; Lu, J.; Mondal, A.; Zaworotko, M. *J. Chem. Commun.* **2001**, 863.
(2) (a) Rowsell, J. L. C.; Yaghi, O. M. *J. Am. Chem. Soc.* **2006**, *128*, 1304. (b) Costes, J. P.; Nicodeme, F. *Chem.—Eur. J.* **2002**, *8*, 3442. (c) Xu, G. F.; Wang, Q. L.; Gamez, P.; Ma, Y.; Clérac, R.; Tang, J.; Yan, S. P.; Cheng, P.; Liao, D. Z. *Chem. Commun.* **2010**, *46*, 1506. (d) Hernández-Molina, M.; Ruiz-Pérez, C.; López, T.; Lloret, F.; Julve, M. *Inorg. Chem.* **2003**, *42*, 5456. (e) Hou, H. W.; Li, G.; Li, L. K.; Zhu, Y.; Meng, X. R.; Fan, Y. T. *Inorg. Chem.* **2003**, *42*, 428. (f) Lee, W. R.; Ryu, D. W.; Lee, J. W.; Yoon, J. H.; Koh, E. K.; Hong, C. S. *Inorg. Chem.* **2010**, *49*, 4723. (g) Zhang, Z. H.; Song, Y.; Okamura, T.; Hasegawa, Y.; Sun, W. Y.; Ueyama, N. *Inorg. Chem.* **2006**, *45*, 2896.

(3) (a) Chen, B. L.; Yang, Y.; Zapata, F.; Lin, G. N.; Qian, G. D.; Lobkovsky, E. B. *Adv. Mater.* **2007**, *19*, 1693. (b) Harbuzaru, B. V.; Corma, A.; Rey, F.; Atienzar, P.; Jorda, J. L.; Garcia, H.; Ananias, D.; Carlos, L. D.; Rocha, J. *Angew. Chem., Int. Ed.* **2008**, *47*, 1080. (c) Xu, H.; Liu, F.; Cui, Y. J.; Chen, B. L.; Qian, G. D. *Chem. Commun.* **2011**, *47*, 3153. (d) Wong, K. L.; Law, G. L.; Yang, Y. Y.; Wong, W. T. *Adv. Mater.* **2006**, *18*, 1051.
(4) (a) Kiritsis, V.; Michaelides, A.; Skoulika, S.; Golhen, S.; Ouahab, L. *Inorg. Chem.* **1998**, *37*, 3407. (b) Long, D. L.; Blake, A. J.; Champness, N. R.; Schröder, M. *Chem. Commun.* **2000**, 1369. (c) Long, D. L.; Blake, A. J.; Champness, N. R.; Wilson, C.; Schroder, M. *J. Am. Chem. Soc.* **2001**, *123*, 3401. (d) Wang, Z.; Jin, C. M.; Shao, T.; Li, Y. Z.; Zhang, K. L.; Zhang, H. T.; You, X. Z. *Inorg. Chem. Commun.* **2002**, *5*, 642.
(5) (a) Férey, G.; Mellot-Draznieks, C.; Serre, C.; Millange, F.; Dutour, J.; Surblé, S.; Margiolaki, I. *Science* **2005**, *309*, 2040. (b) Kesanli, B.; Cui, Y.; Smith, M. R.; Bittner, E. W.; Bockrath, B. C.; Lin, W. B. *Angew. Chem., Int. Ed.* **2005**, *44*, 72.
(6) Pearson, R. G. *J. Am. Chem. Soc.* **1963**, *85*, 3533.
(7) (a) Serre, C.; Férey, G. *J. Mater. Chem.* **2002**, *12*, 3053. (b) Serpaggi, F.; Férey, G. *J. Mater. Chem.* **1998**, *8*, 2749. (c) Serpaggi, F.; Férey, G. *Inorg. Chem.* **1999**, *38*, 4741. (d) Yang, A.−H.; Gao, H.−L.; Cui, J.−Z.; Zhao, B. *CrystEngComm* **2011**, *13*, 1870. (e) Yan, X. H.; Li, Y. F.; Wang, Q.; Huang, X. G.; Zhang, Y.; Gao, C. J.; Liu, W. S.; Tang, Y.; Zhang, H. R.; Shao, Y. L. *Cryst. Growth Des.* **2011**, *11*, 4205. (f) Zhuang, G. L.; Kong, X. J.; Long, L. S.; Huang, R. B.; Zheng, L. S. *CrystEngComm* **2010**, *12*, 2691.
(8) (a) Henry, N.; Costenoble, S.; Lagrenée, M.; Loiseau, T.; Abraham, F. *CrystEngComm* **2011**, *13*, 251. (b) Cai, B.; Yang, P.; Dai, J.-W.; Wu, J.-Z. *CrystEngComm* **2011**, *13*, 985. (c) Cepeda, J.; Beobide, G.; Castillo, O.; Luque, A.; Pérez-Yáñez, S.; Román, P. *Cryst. Growth Des.* **2012**, *12*, 1501.
(9) (a) Beobide, G.; Wang, W. G.; Castillo, O.; Luque, A.; Román, P.; Tagliabue, G.; Galli, S.; Navarro, J. A. R. *Inorg. Chem.* **2008**, *47*, 5267. (b) Beobide, G.; Castillo, O.; Luque, A.; García-Couceiro, U.; García-Terán, J. P.; Román, P. *Dalton Trans.* **2007**, 2669. (c) Beobide, G.; Castillo, O.; Cepeda, J.; Luque, A.; Pérez-Yáñez, S.; Román, P.; Vallejo-Sánchez, D. *Eur. J. Inorg. Chem.* **2011**, 68.
(10) Cepeda, J.; Balda, R.; Beobide, G.; Castillo, O.; Fernández, J.; Luque, A.; Pérez-Yáñez, S.; Román, P.; Vallejo-Sánchez, D. *Inorg. Chem.* **2011**, *50*, 8437.
(11) Hunt, R. R.; McOmie, J. F. W.; Sayer, E. R. *J. Chem. Soc.* **1959**, 525.
(12) Earnshaw, A. *Introduction to Magnetochemistry*; Academic Press: London, 1968.
(13) *CrysAlisPro*, version 1.171.35.15; Agilent Technologies: Yarnton, U.K., 2011.
(14) Altomare, A.; Cascarano, M.; Giacovazzo, C.; Guagliardi, A. *J. Appl. Crystallogr.* **1993**, *26*, 343.
(15) Farrugia, L. J. *J. Appl. Crystallogr.* **1999**, *32*, 837.
(16) Sheldrick, G. M. *Acta Crystallogr.* **2008**, *A64*, 112.
(17) Petricek, V.; Dusek, M.; Palatinus, L. *Jana2006, The Crystallographic Computing System*; Institute of Physics: Praha, Czech Republic, 2006.
(18) (a) Rodríguez-Carvajal, J. *FULLPROF, Program Rietveld for Pattern Matching Analysis of Powder Patterns*; Abstacts of the Satellite Meeting on Powder Diffraction of the XV Congress of the IUCr: Toulouse, France, 1990, 127. (b) Rodríguez-Carvajal, J. *FULLPROF 2000*, version 2.5d; Laboratoire Léon Brillouin (CEA-CNRS), Centre d'Études de Saclay, Gif sur Yvette Cedex: France, 2003.
(19) Zhang, X. M. *Coord. Chem. Rev.* **2005**, *249*, 1201.
(20) (a) Knope, K. E.; Cahill, C. L. *Inorg. Chem.* **2007**, *46*, 6607. (b) Rodríguez-Diéguez, A.; Colacio, E. *Chem. Commun.* **2006**, 4140. (c) Weng, D. F.; Mu, W. H.; Zheng, X. J.; Fang, D. C.; Jin, L. P. *Inorg. Chem.* **2008**, *47*, 1249. (d) Thuéry, P. *CrystEngComm* **2010**, *12*, 1905.
(21) Barrett Adams, D. M. Y.; Kahwa, I. A.; Mague, J. T. *New J. Chem.* **1998**, *22*, 919.
(22) Evans, O. R.; Lin, W. *Cryst. Growth Des.* **2001**, *1*, 9.

(23) (a) Zhang, J. P.; Lin, Y. Y.; Huang, X. C.; Chen, X. M. *Eur. J. Inorg. Chem.* **2006**, 3407. (b) Huh, H. S.; Lee, S. W. *Bull. Korean Chem. Soc.* **2006**, *27*, 1839.

(24) (a) Li, X.; Cao, R.; Sun, D.; Shi, Q.; Bi, W.; Hong, M. *Inorg. Chem. Commun.* **2003**, *6*, 203. (b) Rowland, C. E.; Cahill, C. L. *Inorg. Chem.* **2010**, *49*, 6716. (c) Andrews, M. B.; Cahill, C. L. *CrystEngComm* **2011**, *13*, 7068.

(25) (a) Fujishiro, K.; Mitamura, S. *Bull. Chem. Soc. Jpn.* **1989**, *62*, 786. (b) McNelis, E. *J. Org. Chem.* **1965**, *30*, 1209.

(26) Knope, K. E.; Kimura, H.; Yasaka, Y.; Nakahara, M.; Andrews, M. B.; Cahill, C. L. *Inorg. Chem.* **2012**, *51*, 3883.

(27) (a) Mahata, P.; Prabu, M.; Natarajan, S. *Inorg. Chem.* **2008**, *47*, 8451. (b) Forster, P. M.; Burbank, A. R.; Livage, C.; Férey, G.; Cheetam, A. K. *Chem. Commun.* **2004**, 368.

(28) Shannon, R. D. *Acta Crystallogr.* **1976**, *A32*, 751.

(29) Guzei, I. A.; Wendt, M. *Dalton Trans.* **2006**, 3991.

(30) (a) Llunell, M.; Casanova, D.; Cirera, J.; Bofill, J. M.; Alemany, P.; Alvarez, S.; Pinsky, M.; Avnir, D. *SHAPE (1.7)*; University of Barcelona: Barcelona, 2010. (b) Ruiz-Martínez, A.; Casanova, D.; Alvarez, S. *Chem.—Eur. J.* **2008**, *14*, 1291.

(31) (a) Shi, F.−N.; Cunha−Silva, L.; Trindade, T; Paz, F. A. A.; Rocha, J. *Cryst. Growth Des.* **2009**, *9*, 2098. (b) Li, S.; Chen, Y.; He, H.−M.; Ma, Y.−F. *Acta Crystallogr.* **2009**, *E65*, m411. (c) Huang, Y.−G.; Wu, B.−I.; Yuan, D.−Q.; Xu, Y.−Q.; Jiang, F.−I.; Hong, M.−C. *Inorg. Chem.* **2007**, *46*, 1171.

(32) (a) TOPOS Main Page. http://www.topos.ssu.samara.ru (accessed Nov. 2010). (b) Blatov, V. A. *IUCR CompComm Newsletter*; 2006, p 4.

(33) Spek, A. L. *J. Appl. Crystallogr.* **2003**, *36*, 7.

(34) Infantes, L.; Chisholm, J.; Motherwell, S. *CrystEngComm* **2003**, *5*, 480.

(35) (a) Kahwa, I. A.; Selbin, J.; O'Connor, C. J.; Foise, J. W.; McPherson, G. L. *Inorg. Chim. Acta* **1988**, *148*, 265. (b) Ke, H.; Zhao, L.; Xu, G.−F.; Guo, Y.−N.; Tang, J.; Zhang, X.−Y.; Zhang, H.−J. *Dalton Trans.* **2009**, 10609. (c) Li, B.; Gu, W.; Zhang, L. Z.; Qu, J.; Ma, Z. P.; Liu, X.; Liao, D. Z. *Inorg. Chem.* **2006**, *45*, 10425. (d) Ouyang, Y.; Zhang, W.; Xu, N.; Xu, G. F.; Liao, D. Z.; Yoshimura, K.; Yan, S. P.; Cheng, P. *Inorg. Chem.* **2007**, *46*, 8454. (e) O'Connor, C. J. *Prog. Inorg. Chem.* **1982**, *29*, 203.

(36) (a) Li, Y.; Zheng, F. K.; Liu, X.; Zou, W. Q.; Guo, G. C.; Lu, C. Z.; Huang, J. S. *Inorg. Chem.* **2006**, *45*, 6308. (b) Andruh, M.; Bakalbassis, E.; Kahn, O.; Trombe, J. C.; Porcher, P. *Inorg. Chem.* **1993**, *32*, 1616. (c) Wang, Y.; Li, X. L.; Wang, T. W.; Song, Y.; You, X. Z. *Inorg. Chem.* **2010**, *49*, 969.

(37) (a) Curély, J. *Europhys. Lett.* **1995**, *32*, 529. (b) Curély, J. *Physica B* **1998**, *245*, 263. (c) Delgado, F. S.; Kerbellec, N.; Ruiz-Pérez, C.; Cano, J.; Lloret, F.; Julve, M. *Inorg. Chem.* **2006**, *45*, 1012.

(38) (a) Hemmilä, I. *J. Alloys. Compd* **1995**, *225*, 480. (b) Moynagh, J.; Schimmel, H. *Nature* **1999**, *400*, 105.

(39) Desurvire, E. *Phys. Today* **1994**, *47* (1), 20.

(40) Baldo, A. M.; Thompson, M. E.; Forrest, S. R. *Pure Appl. Chem.* **1999**, *71*, 2095.

(41) (a) Janiak, C. *Dalton Trans.* **2003**, 2781. (b) Bünzli, J. C. G.; Eliseeva, S. V. *J. Rare Earths* **2010**, *28*, 824.

(42) Bünzli, J. C. G. *Lanthanide Probes in Life, Chemical, and Earth Sciences: Theory and Practice*; Elsevier Science Publications: Amsterdam, 1989.

(43) Yen, W. M.; Shionoya, S.; Yamamoto, H. *Phosphor Handbook*; CRC Press: Athens, 2007.

(44) (a) Bhaumik, M. L. *J. Chem. Phys.* **1964**, *40*, 3711. (b) Sabbatini, N.; Guardigli, M.; Manet, I. *Adv. Photochem.* **1997**, *23*, 213. (c) Prodi, L.; Maestri, M.; Balzani, V.; Lehn, J. M.; Roth, C. *Chem. Phys. Lett.* **1991**, *180*, 45.

(45) Sabbatini, N.; Perathoner, S.; Lattanzi, G.; Dellonte, S.; Balzani, V. *J. Phys. Chem.* **1987**, *91*, 6136.

(46) (a) Kropp, J. L.; Windsor, M. W. *J. Chem. Phys.* **1965**, *42*, 1599. (b) Horrocks, W. D.; Sudnick, D. R. *Acc. Chem. Res.* **1981**, *14*, 384.

(47) Beeby, A.; Clarkson, I. M.; Dickins, R. S.; Faulkner, S.; Parker, D.; Royle, L.; de Sousa, A. S.; Williams, J. A. G.; Woods, M. *J. Chem. Soc., Perkin Trans. 2* **1999**, 493.

7888

dx.doi.org/10.1021/ic3009392 | *Inorg. Chem.* 2012, 51, 7875−7888